IEEE Access
Multidisciplinary | Rapid Review | Open Access Journal

Received July 2, 2021, accepted July 20, 2021, date of publication July 26, 2021, date of current version August 6, 2021.

Digital Object Identifier 10.1109/ACCESS.2021.3099986

What Is the Role of Frequency on Neural Activation in Tonic Stimulation in SCS Therapy? A Computational Study on Sensory Aβ Nerve Fibers

CARMEN SOLANES[1], JOSÉ L. DURÁ[1], (Member, IEEE), JOSE DE ANDRÉS[2,3], AND JAVIER SAIZ[1]

[1]Center of Research and Innovation in Bioengineering (Ci2B), Universitat Politècnica de València, 46022 Valencia, Spain
[2]Anesthesia, Critical Care, and Multidisciplinary Pain Management Department, General University Hospital, 46017 Valencia, Spain
[3]Surgical Specialties Department, Anesthesia Unit, Valencia University Medical School, 46010 Valencia, Spain

Corresponding author: Carmen Solanes (carsogal@etsii.upv.es)

ABSTRACT The investigation of the effect of the stimulation parameters by computational modeling helps to understand the electrical response of specific neural elements in Spinal Cord Stimulation (SCS) therapy for chronic pain treatment. While the effect of the amplitude, the pulse width, and the electrode configuration on neural activation has been widely studied and is well-established in tonic stimulation, how frequency influences neural activation remains unclear. Thus, the aim of this work is to study the effect of frequency on the electrical response of sensory Aβ neurons in tonic stimulation. Our approach consisted of the development of a new nerve fiber model from the combination of two previous models used in SCS modeling (the Wesselink-Holsheimer-Boom model and the Richardson-McIntyre-Grill model B). We simulate the action potential and the gates probabilities evolution of a 12.8 μm fiber diameter at different pulse frequencies (50, 350, 600, 800, and 1000 Hz). We also simulated the firing rate of two nerve fiber diameters (5.7 and 12.8 μm) in function of pulse frequency (from 1 to 1400 Hz) at different pulse widths (100, 300, and 500 μs). In the range of 2-1000 Hz, the firing rate of a 12.8 μm-diameter nerve fiber can be maximized by utilizing a 350 Hz, 300 μs-stimulus. Frequencies above 350 Hz reduce half to one-third the firing rate, and 1000 Hz-stimulus overrides the electrical activity of the sensory nerve fiber. Small fibers (5.7 μm-diameter) present lower firing rate values than large fibers (12.8 μm-diameter). High values of pulse width decrease the firing rate of the nerve fibers as well as the range of frequencies that could be used to stimulate. According to the results, the frequency could have a considerable implication on the modulation of the firing rate of a nerve fiber. Thus, the frequency could play an important role to select and increase the activity of specific neural elements of the spinal cord in SCS therapy.

INDEX TERMS Aβ nerve fibers, pulse frequency, sensory nerve fiber model, spinal cord stimulation therapy, tonic stimulation.

I. INTRODUCTION

Spinal Cord Stimulation (SCS) consists of delivering electrical pulses to a targeted spinal cord area using leads placed in the epidural space (a few levels above the affected spinal segments) that are connected to a neurostimulator [51]. This therapy has demonstrated to be effective for the management of several neuropathic pain conditions, such as peripheral vascular disease, failed back surgery syndrome, or complex regional pain syndrome, among others [33], [48], [71], and for motor rehabilitation, such as the recovery of functional walking, and restoration of dormant motor and autonomic supraspinal pathways [10], [13], [23]. Despite the substantial clinical benefits of SCS therapy for chronic pain treatment [19], [34], [35], [66], the neurophysiological mechanisms involved in SCS are still not well-known. Nevertheless, the gate-control pain theory proposed by Melzack and Wall is the one most accepted to explain the basis of SCS

The associate editor coordinating the review of this manuscript and approving it for publication was Yizhang Jiang.

therapy for tonic stimulation [11]. This theory explains that electrical activation of large, myelinated mechanoreceptor afferents (Aβ fibers) indirectly modulates the transmission of painful information from small, unmyelinated afferents (C fibers) within the dorsal horn [25], [49], [51], [53]. Moreover, some studies affirm that the aim of SCS is to activate dorsal columns, which contains axons that originate in the large-diameter afferent sensory nerve fibers, i.e. afferent Aβ neurons [22], [26].

During the last 40 years, spinal cord stimulation modeling studies have been used for understanding the effect of the stimulation parameters (amplitude, pulse width, polarity and frequency), such as Lee *et al.* [36], that predicted greater activation of medial dorsal column fibers with increased pulse width, which correlated with a clinical study from Yearwood *et al.* [24]; Holsheimer and Wesselink [27], who observed the major determinant of dorsal column and dorsal root activation is electrode polarity; and Durá *et al.* [17], that predicted higher dorsal column fibers activation with dual-guarded cathode polarity. As for frequency, the recent growing use of new stimulation strategies in clinical practice, such as 10 kHz [31], [72] and burst stimulation [16], [58], has increased the interest of studying, by computational modeling, the effect of high-frequency stimulation on Aβ fibers electrical response, despite the limitation that the mechanisms of actions are still not well-understood for these types of stimulation [5], [37], [42]. However, although the mechanisms of actions are well-known for tonic stimulation [11], [42], [50], [73], little is known about how ''low'' frequency stimulation management affects sensory Aβ nerve fibers activation.

Frequencies between 2-1,200 Hz can be delivered by most neurostimulators [75]. However, tonic stimulation usually applies an electrical stimulus with a ''low'' frequency that ranges between 40-60 Hz, a pulse width of 150-500 μs, and amplitude producing comfortable tingling sensation (paresthesia) in the painful area of the patient [11], [38], [42], [50]. Several studies show that different type of neurons could likely entrain electrical stimulation below 200 Hz [6], [8], [70], end even at 900 Hz [50].

The goal of this work is to study the electrical response of sensory Aβ nerve fibers to different frequencies that are available in tonic stimulation. To achieve this, we present a new sensory nerve fiber model based on electrophysiological and morphometric data for human sensory nerve fibers. Then, by computational modeling, we simulate the action potential and the evolution of the gates' probabilities of the ionic channels to investigate the effect of frequency on the firing rate of a nerve fiber. Finally, we also study the electrical response of two nerve fiber diameters (5.7 and 12.8 μm).

II. METHODS

A. NEW SENSORY NERVE FIBER

The new sensory nerve fiber is a combination of the Wesselink-Holsheimer-Boom (WHB) sensory nerve fiber model and the Richardson-McIntyre-Grill (RMG) motor nerve fiber model B. The parameters of membrane kinetics were taken from [76], which are described in Appendix. The values of the electrical parameters of the nodal and internodal (myelin) compartments are shown in Table 1. To yield an action potential shape that includes hyperpolarizing afterpotential that matches experimental data from the electrical behavior of sensory nerve fibers, the following parameters of the model were adjusted.

TABLE 1. Electrical parameters of the new sensory nerve fiber model.

Symbol	Parameter	Value	Unit
p_{Na}	Na^+ channel permeability	$7.04{\cdot}10^3$	$cm{\cdot}s^{-1}$
g_K	Slow K^+ channel conductivity	30	$mS{\cdot}cm^{-2}$
g_{Lk}	Leak channel conductivity	60	$mS{\cdot}cm^{-2}$
$[Na]_{out}$	Na^+ channels extracellular concentration	154	mM
$[Na]_{in}$	Na^+ channels intracellular concentration	30	mM
F	Faraday constant	96485	C/mol
R	Gas constant	8314.4	mV/K mol
T	Temperature	310.15	K
E_K	K^+ channel equilibrium potential	-84	mV
E_{Lk}	Leak channel equilibrium potential	-84.14	mV
V_{rest}	Resting potential	-84	mV
ρ_{ax}	Axoplasmic resistivity	70	Ωcm
ρ_{ex}	External resistivity	300	Ωcm
c_n	Specific nodal capacitance	2	$\mu F{\cdot}cm^{-2}$
c_m	Specific myelin capacitance	0.1	$\mu F{\cdot}cm^{-2}$
g_m	Specific myelin conductance	1	$mS{\cdot}cm^{-2}$

The axoplasmic resistivity (ρ_{ax}) is shown to produce significant changes in conduction velocity (CV) values [60]. The WHB model has a ρ_{ax} value of 33 $\Omega{\cdot}$cm. In our model, this value was increased to 70 $\Omega{\cdot}$cm to match CV values to experimental data for fiber diameters ranging from 5.7 to 16 μm. On the other hand, to avoid spontaneous firing and match the action potential characteristics to experimental data, the membrane kinetics was calibrated by adjusting the sodium activation and inactivation gate coefficients (α_{m} and α_{h}, respectively). Therefore, we used the α_{m} and α_{h} voltage and time-dependent parameters obtained from the Howells model for sensory nerve fibers (see Appendix) [28].

In Fig. 1, the electrical diagram of the new sensory nerve fiber model is presented. As the figure shows, the internode (myelin) is modeled as in the RMG model B, represented by a conductance connected to a capacitor in parallel. In this manner, the myelin behaves as an imperfect insulator, which means that current losses are considered. On the other hand, the model of the nodes of Ranvier includes three ionic currents: sodium current, fast potassium current, and leakage current. The equations of the ionic currents, the myelin parameters, and the gates' probabilities of the ionic channels are shown in Appendix.

Applying Kirchhoff's law, the membrane currents at each compartment n is equal to the sum of the incoming axial currents and to the sum of the capacitive and ionic currents (if the compartment is a node of Ranvier) through the membrane. Thus, two first-order differential equations are required: one for nodal compartments (1) and one for

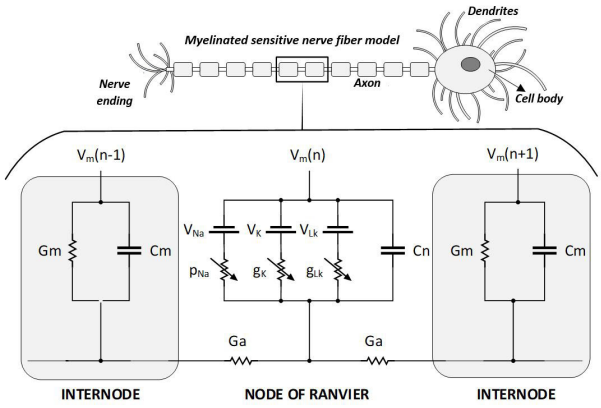

FIGURE 1. Electrical diagram of the new sensitive nerve fiber model.

internodal compartments (2):

$$\frac{dV_n}{dt} = (G_a(V_{m,n-1} - 2V_{m,n} + V_{m,n+1} + V_{e,n-1} - 2V_{e,n} + V_{e,n+1}) - \pi dlI_{ion,n})/C_n \quad (1)$$

$$\frac{dV_n}{dt} = (G_a(V_{m,n-1} - 2V_{m,n} + V_{m,n+1} + V_{e,n-1} - 2V_{e,n} + V_{e,n+1}) - G_m(V_{m,n} - V_{rest}))/C_m \quad (2)$$

where G_a is the axial conductance between two compartments (mS), C_n is the nodal membrane capacitance (mF), G_m is the myelin membrane conductance (mS), C_m is the myelin membrane capacitance (mF), $V_{m,n}$ is the membrane potential value at n compartment (mV), d is the nodal diameter (cm), l is the nodal length (cm), $I_{ion,n}$ is the sum of the ionic currents at n nodal compartment (mA/cm^2), V_{rest} is the resting potential (mV) and $V_{e,n}$ is the external electric potential in n compartment (mV). A complete description of these parameters is presented in Appendix. The total number of differential equations to be solved depends on the number of nodes of Ranvier we consider the nerve fiber has.

B. OUTPUT PROCESSING

Several parameters were calculated using the new nerve fiber model to characterize the simulated action potential.

The amplitude of the action potential corresponded to the absolute value measured from the resting potential up to the peak amplitude.

CV was used to compare the behavior of the model with experimental data. It was measured from two consecutive nodes of Ranvier with a stimulus amplitude of 1.2 the voltage threshold (V_{th}).

Chronaxie was also measured and compared to experimental data values. Chronaxie value corresponded to the stimulation pulse width needed to activate a nerve fiber at 2 V_{th}. V_{th} is first measured using a pulse width of 1500 μs.

Absolute and relative refractory periods were also calculated using the new nerve fiber model to characterize the refractory behavior of the model. Hence, to produce an initial action potential, a stimulation pulse width of 100 μs and an amplitude of 20% above of the V_{th} were used. Then, to elicit a second action potential, the same pulse width of 100 μs was used, but the amplitude was risen to 4 V_{th}. Thus, the absolute refractory period corresponded to the maximum interval between two pulses in which no second potential can be produced; and the relative refractory period corresponded to the maximum interval in which an elevated stimulus was required to elicit a second propagating action potential [76].

Finally, we simulated the evolution of the membrane potential and the gates' probabilities of the ionic channels to study the electrical response of a nerve fiber at 50, 350, 600, 800, and 1000 Hz pulse frequencies with a pulse width of 300 μs. Moreover, the firing rate of 5.7 and 12.8 μm-diameter nerve fibers was calculated in the range of 1-1400 Hz-stimulus with a pulse width of 100, 300, and 500 μs.

III. RESULTS

A. NERVE FIBER MODEL

1) SHAPE OF THE ACTION POTENTIAL

The simulated action potential obtained from the new sensory nerve fiber model can be seen in Fig. 2. The characteristics measured from the simulation of the action potential were compared against the values estimated from experimental data (see Table 2).

TABLE 2. Characteristics of the new sensory nerve fiber model and experimentally determined characteristics of myelinated nerve fibers. Calculated values with monopolar stimulus of 100 μs of pulse width; 12.8 μm nerve fiber diameter and 0.5 mm of distance between the electrode and the nerve fiber. DC: dorsal column; WM: white matter.

Parameter	New model values	Experimental data values		Specifications of the experimental data
Amplitude (mV)	108.5	117	[64]	Human, 25°C of temperature
Conduction velocity (m/s)	50	25−65	[59]	Mammalian, DC myelinated axons, WM
		25−70	[74]	Human sural nerve, body temperature
Chronaxie(μs)	103	70−90	[59]	Mammalian, DC myelinated axons, WM
		106−400	[56]	Rat brain, myelinated axons, WM
Absolute Refractory Period (ms)	1.23	0.58−0.79	[69]	Human sensory nerve fibers
Relative Refractory Period (ms)	2.42	2−3.95	[69]	Human sensory nerve fibers

We first calculated the action potential amplitude. For this parameter, we obtained a value of 108.5 mV. Experimentally, the action potential amplitude in human nerve fibers is around 117 mV, according to Schwarz *et al.* [64]. However, this experimental value corresponded to an action potential produced from a nerve fiber at 25°C and not at body temperature (37°C).

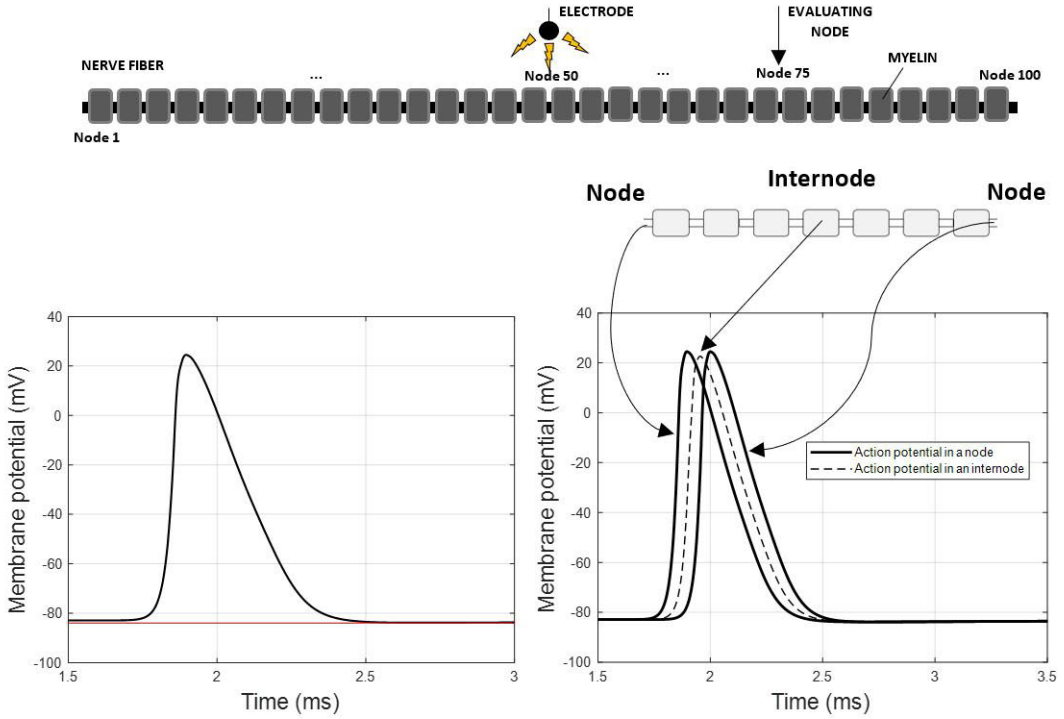

FIGURE 2. Simulated action potentials at 37°C obtained with the new model (left). The horizontal line represents the rest potential considered (−84 mV); and action potential propagation through two nodes of ranvier and one internode located between them (right). A nerve fiber of 12.8 μm in diameter was stimulated with a stimulus of 300 μs of pulse width and an amplitude of 1.2 V_{th}. A separation of 6 nodes of ranvier between the two nodes was selected to clearly see the action potential propagation. The internode that was just in the middle of the two selected nodes was the one whose action potential is represented in the graph.

As for CV, the new nerve fiber model presented a value that was within the physiologic range (25-70 m/s) obtained from several experimental studies [54], [59], [62], [74]. CV depends directly on nerve fiber diameter; thus, CV increases with fiber diameter. In this case, the value obtained (50 m/s) corresponded to a 12.8 μm-diameter nerve fiber.

Chronaxie values were also calculated. Here, experimental data from mammalian myelinated axons show chronaxie values in the range of 70-90 μs [56], while the experimental range of myelinated axons from rat brain is 106-400 μs [56]. The developed nerve fiber model presented a chronaxie value of 103 μs, a value 14.44% higher than the maximum value of the experimental range mammalian DC myelinated axons (90 μs) [59], and 2.9% lower than the minimum value of the experimental data from rat brain [56].

The absolute and the relative refractory periods (ARP and RRP, respectively) were also measured. ARP was 1.23 ms, which is close to the maximum value of the experimental range (0.79 ms). And RRP was 2.42 ms, a value that is within the experimental range (2-3.95 ms) measured from human sensory nerve fibers [69]. Therefore, the refractoriness of the developed sensory nerve fiber model fits sensory human nerve fibers experimental data.

The propagation of the action potential through the myelin compartment of the nerve fiber was also simulated (see Fig. 2). The myelin is modeled as an imperfect insulator and, when the action potential is propagated through the myelin, current losses are produced. The action potential amplitude is 108.5 mV in the first node of Ranvier but, in the myelin compartment, the amplitude is decreased to 106.7 mV (1.66% lower). Then, when the action potential is propagated to the following node of Ranvier, the amplitude value remains as in the previous node of Ranvier (108.5 mV). Thus, the figure shows that current losses are produced at every internode compartment.

Fig. 3 shows the action potential shape of the WHB model and the new nerve fiber model during the afterpotential of a 12.8 μm-diameter fiber.

The figure reveals that neither depolarizing afterpotential nor hyperpolarizing are generated in the WHB model. Therefore, when the action potential is over, the membrane potential is maintained at the initial resting potential (−84 mV), showing no voltage fluctuations. Nevertheless, the new nerve fiber model developed generates a hyperpolarizing afterpotential. In this case, the membrane voltage reaches 0.88 mV below resting potential immediately following the action potential, then rising gradually back to the resting potential (−84 mV). This voltage fluctuation had a duration of 5.3 ms. From experimental data, it is shown that motor nerve fibers generate a depolarizing afterpotential following the action potential [14], while sensory nerve fibers produce

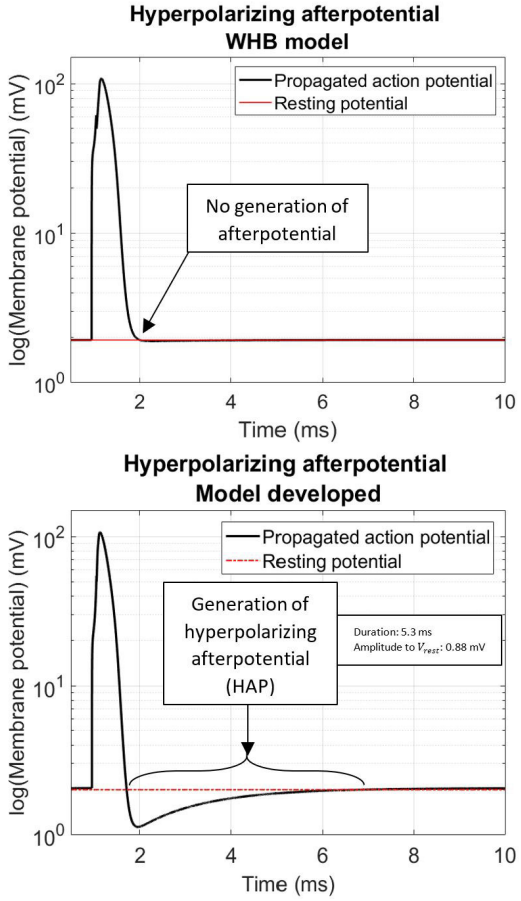

FIGURE 3. Hyperpolarizing afterpotentials obtained with the wesselink-holsheimer-boom nerve fiber model (above), and the new nerve fiber developed (below). The curves of the models' response shown are semilog plot of the action potential. The electric response corresponds to a 12.8 μm-diameter nerve fiber stimulated with a 100 μs-duration monophasic rectangular pulse. Electrode is located 0.5 mm from the middle of the axon.

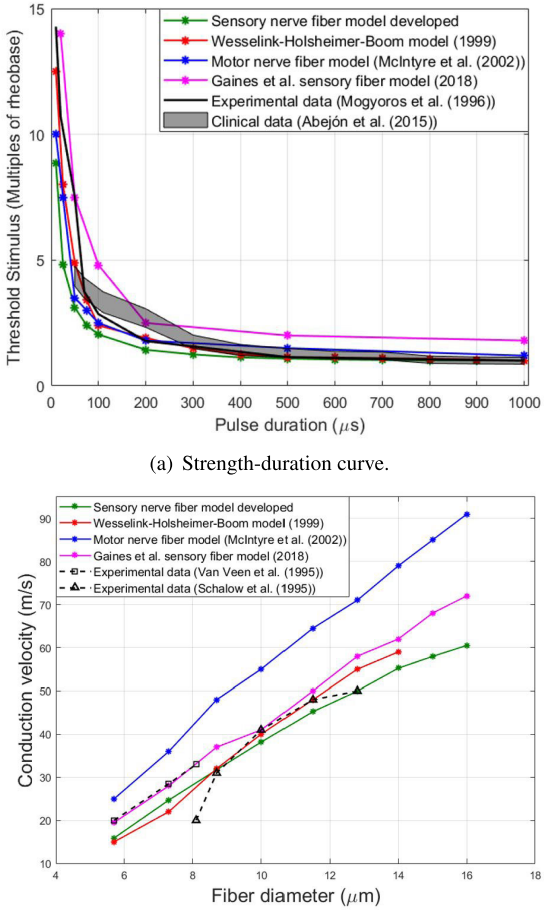

(a) Strength-duration curve.

(b) Conduction velocity for different fiber diameters.

FIGURE 4. a) Strength-duration curve of the developed model compared to WHB model [76], MRG model [46], Gaines *et al.* model [21], experimental data (Mogyoros *et al.* [52]) and clinical (Abejón *et al.* [1]). b) Conduction velocity for different fiber diameters (5.7-16 μm) of the developed model, WHB model [76], MRG model [46], Gaines *et al.* model [21], and experimental data from Van Veen *et al.* [74] and Schalow *et al.* [63].

a hiperpolarizing afterpotential [67]. Therefore, the afterpotential generated by the new nerve fiber model behaves as a sensory nerve fiber.

On the other hand, differences between the action potential durations were also observed. The action potential in the WHB model had longer duration than the new nerve fiber model (1 versus 0.8 ms, respectively). Experimental recordings showed an action potential duration of 2.6 ms. Thus, both the WHB and the new nerve fiber model action potentials were shorter than the experimental data (56.5 and 65.2% lower, respectively).

2) STRENGTH-DURATION CURVE AND CONDUCTION VELOCITY

The strength-duration and CV-diameter curves were generated for the new nerve fiber model and compared to experimental data and previous nerve fiber models (WHB sensory model, MRG motor model, and Gaines *et al.* sensory model).

The strength-duration curve was normalized to the rheobase voltage, as shown in Fig. 4. The new nerve fiber model data presents a similar shape to curves obtained with previous nerve fiber models, experimental data, and clinical. The developed model shows lower stimulation threshold values than the experimental, clinical data, and the other computational models for pulse durations below 400 μs. For instance, for 100 μs-duration, threshold stimulus in the developed model is 28.42 and 38.2% lower than the experimental and the clinical data (2.04 versus 2.85, and 3.3 the rheobase voltage, respectively), while Gaines *et al.* model has a threshold stimulus that is 45 and 68.4% higher (4.8 versus 2.85, and 3.3 the rheobase voltage, respectively). The WHB sensory fiber model and the MRG motor fiber model present values that are 17.6 and 22.5% higher than the threshold stimulus obtained with the developed model (2.4 and 2.5 versus 2.04 the rheobase voltage, respectively).

The CV-diameter curve also presents differences between the nerve fiber developed and previous nerve fiber models (see Fig. 4). Comparing to the MRG motor fiber model,

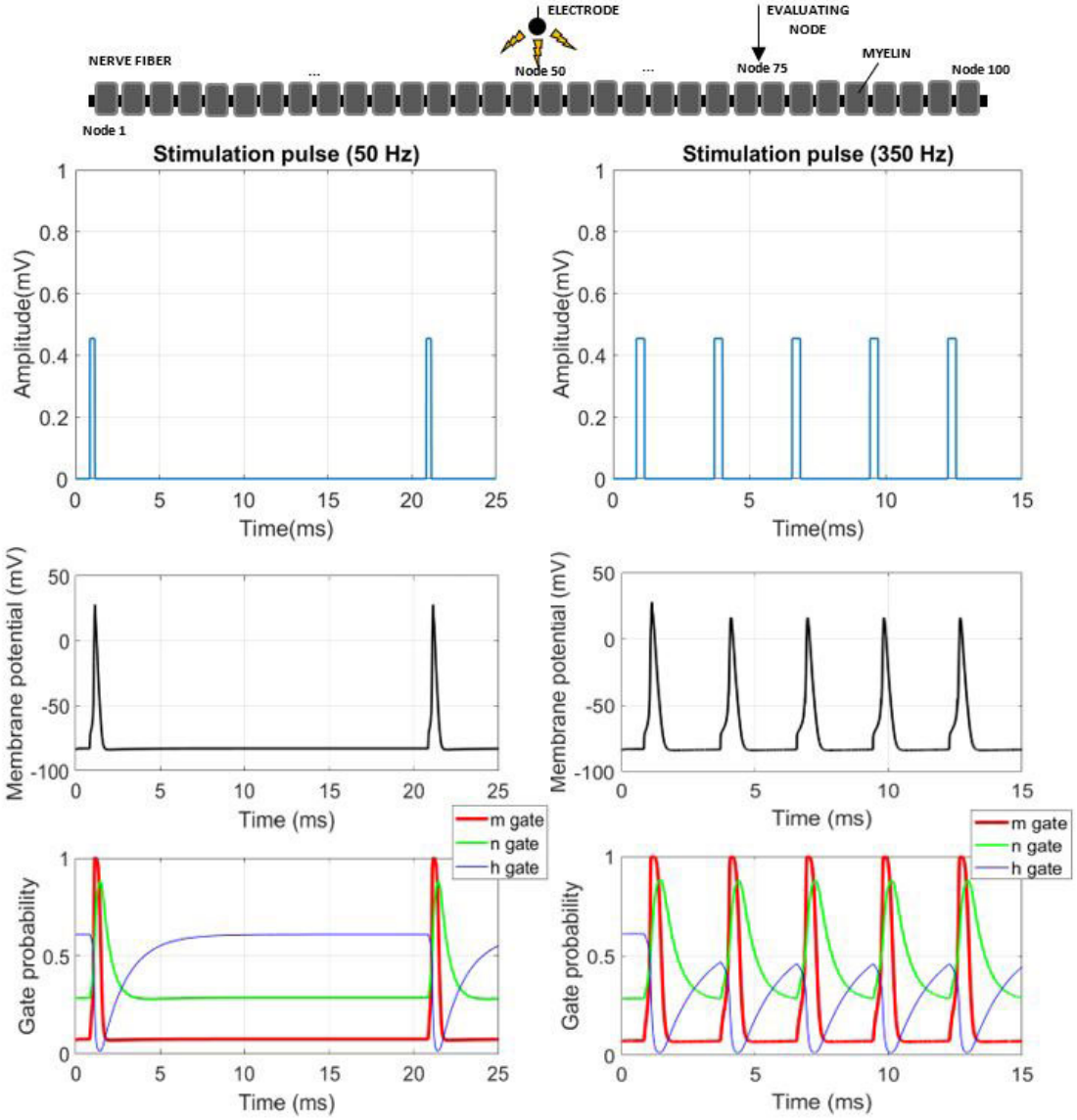

FIGURE 5. Electric response of a 12.8 μm nerve fiber during a stimulus with a frequency of 50 Hz (left) and 350 Hz (right), and pulse width of 300 μs. The figures above show the stimulus pattern applied. The figures below show the action potential and the evolution of the gates' probabilities in the node 75 of the nerve fiber at each pulse stimulus. The amplitude applied is 1.2 V_{th} (threshold stimulus). Electrode is located at 0.5 mm from the middle of the axon.

the three sensory nerve fiber models (the WHB model, Gaines *et al.* model, and the new model developed) show lower CV for all fiber diameters considered (5-16 μm), which matched better to the experimental data obtained from sensory fibers [63], [74]. The CV values from 5.7 to 8 μm in Gaines *et al.* model and the developed model were lower than the experimental data from Van Veen *et al.* [74]. However, in the range of 8.7-12.8 μ, both models fitted well to experimental data from Schalow *et al.* [63]. Instead, the WHB model fitted well to Van Veen *et al.* experimental data [74], showing slight higher CV values than experimental data at higher fiber diameters.

B. EFFECT OF FREQUENCY ON NERVE FIBER ACTIVATION

In this study, several stimulation frequencies (50, 350, 600, 800, and 1000 Hz) were considered to simulate the action potential and the gates' probabilities of the ionic channels of a 12.8 μm nerve fiber diameter. A common frequency used in tonic stimulation for SCS therapy is 50 Hz. As shown in Fig. 5, when a 50 Hz stimulus is applied, an action potential every pulse is obtained. At each pulse, the gates' probabilities of sodium (m and h gates) and potassium (n gate) channels are ready to electrically depolarize the axon. The time between pulses (20 ms) is higher than the refractory period of the nerve fiber (2.42 ms), so the gates of the ionic channels have enough

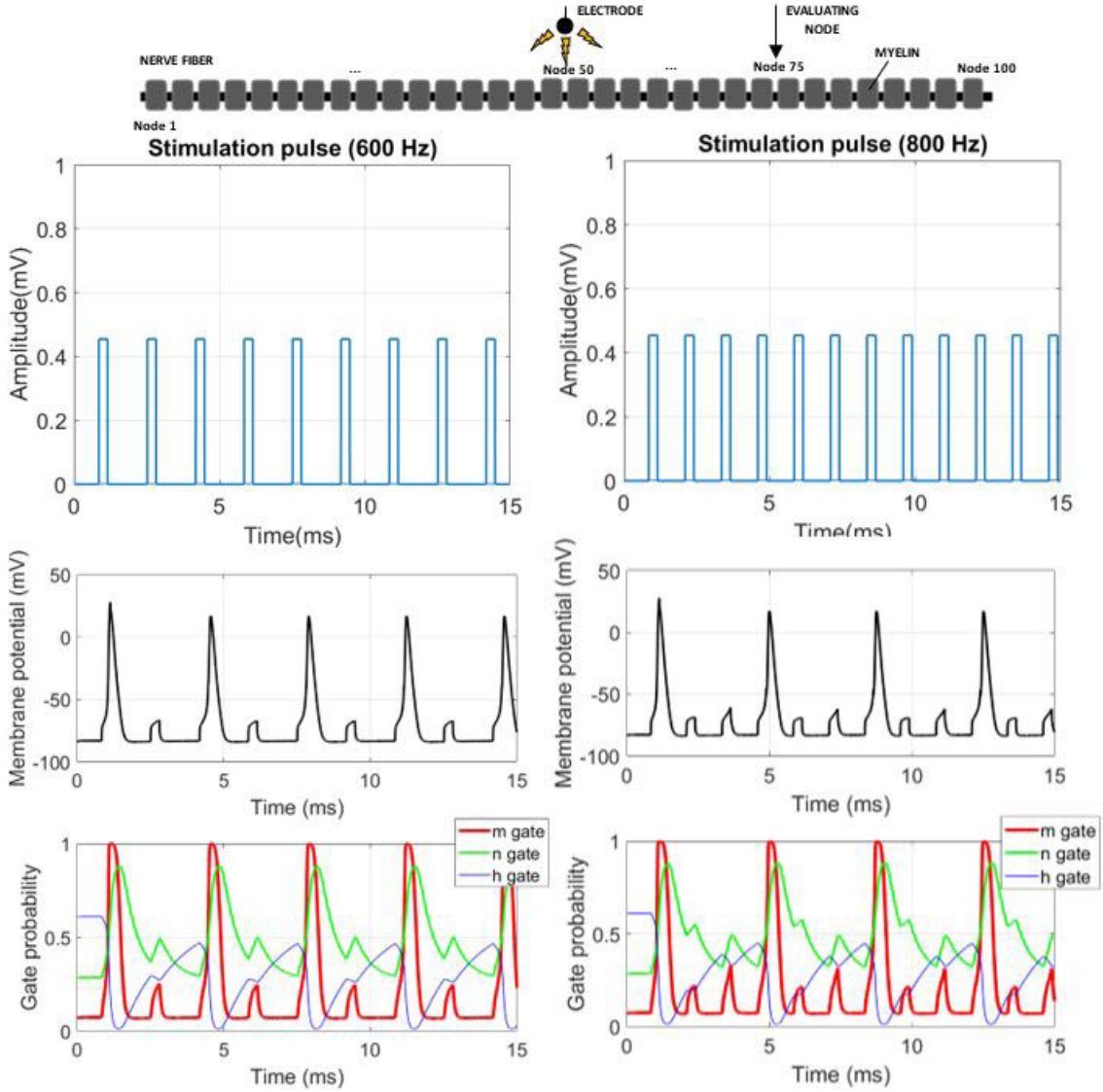

FIGURE 6. Electric response of a 12.8 μm nerve fiber during a stimulus with a frequency of 600 Hz (left) and 800 Hz (right), and pulse width of 300 μs. The figures above show the stimulus pattern applied. The figures below show the action potential and the evolution of the gates' probabilities in the node 75 of the nerve fiber at each pulse stimulus. The amplitude applied is 1.2 V_{th} (threshold stimulus). Electrode is located at 0.5 mm from the middle of the axon.

time to recover and are available to be activated again at the next stimulation pulse.

When the stimulation frequency is increased to 350 Hz, an action potential per pulse is also obtained (see Fig. 5). In this case, the gates' probabilities of the ionic channels are not totally recovered when the next pulse is applied, since the time between pulses is 11.6% lower than the relative refractory period (2.7 versus 2.42 ms), and 119.5% higher than the absolute refractory period (2.7 versus 1.23 ms). As shown in Fig. 5, at the time the second pulse starts, m gate (sodium channel) and n gate (potassium channel) are totally recovered, but h gate has a value of 0.469, i.e. it is 76.94% recovered, which means that the nerve fiber is still in the refractory state. However, the stimulus amplitude applied (1.2 V_{th}) is strong enough to depolarize the axon again, generating an action potential every pulse.

Fig. 6 reveals that at a frequency of 600 Hz the firing rate of the nerve fiber is reduced by half (300 Hz) i.e., an action potential is obtained every two pulses. Here, after the first pulse, the axon is depolarized, and then the recovery cycle starts. For this stimulation frequency, the time between pulses is 1.67 ms, which is 35.8% higher than the absolute refractory period (1.23 ms) and 31% lower than the relative refractory period (2.42 ms). Although the nerve fiber would be in the refractory state, now the amplitude applied (1.2 V_{th}) is not strong enough to produce another axon depolarization in the second pulse. As shown in Fig. 6, m gate (sodium channel) is recovered, but n gate (potassium channel) has

a value of 0.3698 and h gate (sodium channel) is 0.2946, being at 71.28% and 48.3% of their recovery, respectively. Instead, when the third pulse starts, the recovery cycle has progressed; m and n gates of the ionic sodium and potassium channels are recovered while h gate is almost at their initial value (0.4664 versus 0.6096), thus an action potential can be generated again.

On the other hand, with an 800 Hz-stimulus, the sensory fiber is depolarized every three pulses, producing a firing rate that is reduced to one third of the stimulation frequency (see Fig. 6). In this scenario, the time between pulses is 1.25 ms, which is 1.63% higher than the absolute refractory period (1.23 ms) and 51.65% lower than the relative refractory period (2.42 ms). The evolution of the gates' probabilities shows that at the first pulse the action potential is produced. When the second pulse is applied, the fiber had not enough time to recover and leave from the absolute refractory period. Although m gate (sodium channel) is recovered, n gate (potassium channel) and h gate (sodium channel) are still at 28.6% (0.4924) and 32.46% (0.197) of their initial values (0.2873 and 0.6096, respectively), hence no depolarization is produced. At the third pulse, the gates of the ionic channels had more time to recover. As the second pulse did not generate an action potential, the axon is now more excitable. The time between the third and the first pulses is 2.5 ms, which means that the nerve should have finished the recovery cycle (the relative refractory period is 3.3% lower than the time between pulses (2.42 versus 2.5 ms)). However, although the second pulse did not generate an action potential, the gates' probabilities were slightly reverted. Hence, at the third pulse, m gate is totally recovered, n gate value is almost at its initial value (0.3204 versus 0.2873, respectively), and h gate recovery has increased to 64.1%. In this case, the stimulation amplitude is not high enough, thus an action potential is not produced. But, at the fourth pulse, although the recovery cycle is not finished yet (m and n gates are recovered, but h gate is at 74% of its recovery), the time between the first and fourth pulses is 3.75 ms, which is about 55% higher than the relative refractory period (2.42 ms), thus the nerve fiber is not in the refractory state and it can be depolarized again.

The electrical response of a sensory nerve fiber to a 1000 Hz-stimulus is shown in Fig. 7. The figure reveals that after the first pulse depolarization, no more action potential can be generated again. The time between pulses is 1 ms, which is 18.7% lower than the absolute refractory period (1.23 ms). At the second pulse, the fiber is still in the absolute refractory period, and the stimulus cannot elicit an action potential. At the third pulse, the nerve fiber would be in the refractory state. But, although the gates have partly recovered, the stimulus is not strong enough to depolarize the fiber. From this point, Fig. 7 shows that the recovery of the ionic channels gates is slower than in previous pulses. As there is only 1 ms between pulses, the fiber has no time to advance in the refractory state i.e., the recovering produced between pulses is always reverted by the stimulation pulse. Although m gate recovers completely, n gate and h gate recover a

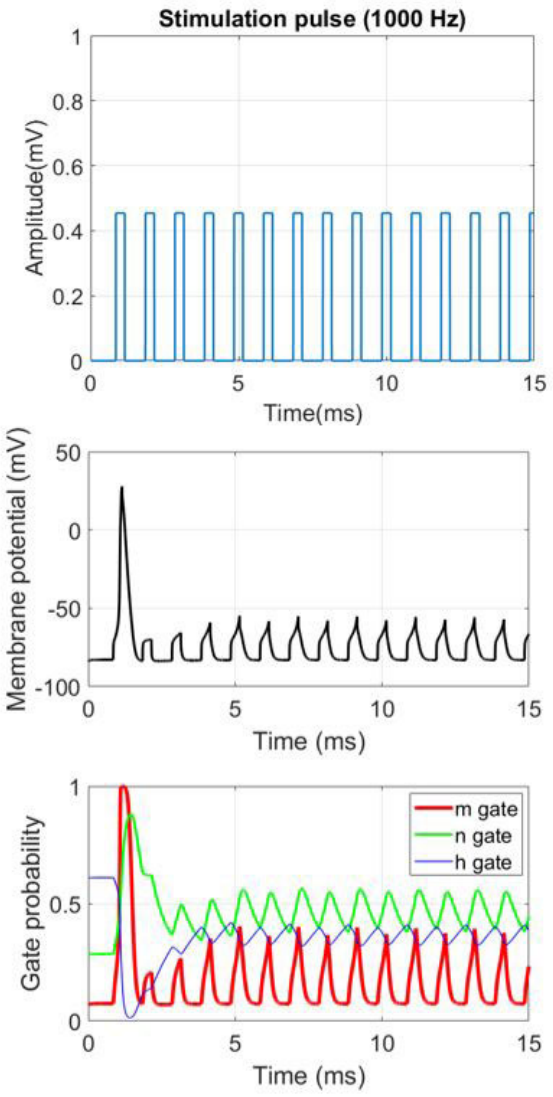

FIGURE 7. Electric response of a 12.8 μm nerve fiber during a stimulus with a frequency of 1000 Hz and pulse width of 300 μs. The figure above show the stimulus pattern applied. The figure below show the action potential and the evolution of the gates' probabilities in the node 75 of the nerve fiber at each pulse stimulus. The amplitude applied is 1.2 V_{th} (threshold stimulus). Electrode is located at 0.5 mm from the middle of the axon.

maximum of 81% and 68.72%, respectively. Owing to the fact that the fiber cannot enter an excitable state as well as the stimulus amplitude is not sufficient to depolarize the nerve fiber, the rest of pulses do not generate action potentials, and the firing rate of the nerve fiber is overridden.

C. PATTERNS OF ACTIVITY AND NERVE FIBER DIAMETER

According to a histological study from Feirabend *et al.* [18], the largest fibers that can be recruited in the medial DC have a diameter of 12 μm. However, the maximum fibers density in the medial DC corresponds to fibers diameters < 7.1 μm. As there are available data for the geometric parameters of 5.7 and 12.8 μm-diameter fibers [46], and previous computational models also considered these fiber

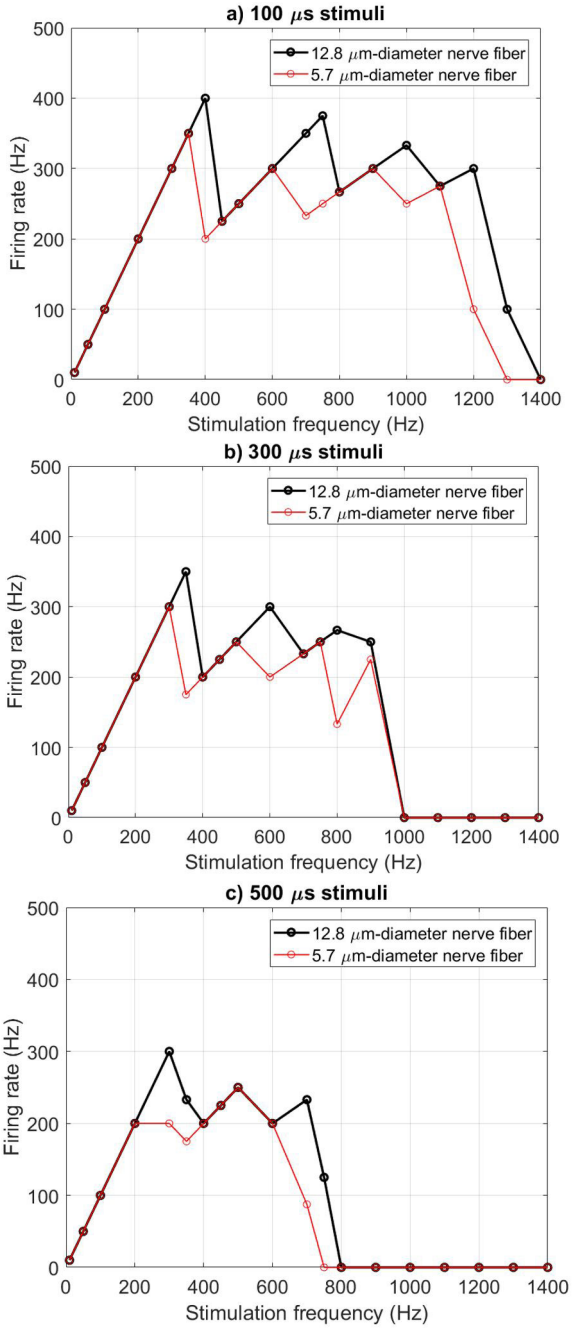

FIGURE 8. Firing rate in function of stimulation frequency for 5.7 and 12.8 μm-diameter nerve fiber when applying a pulse width stimuli of: a) 100 μs; b) 300 μs; and c) 500 μs. The nerve fibers are stimulated with a rectangular monophasic pulse, and an amplitude of 1.2 V_{th} (threshold stimulus). Electrode is located at 0.5 mm from the middle of the axon.

diameters [37], [39], [68], we simulated the activation pattern of a 5.7 and 12.8 μm-diameter nerve fiber in function of the stimulation frequency at different pulse widths: 100, 300, and 500 μs.

Fig. 8 shows that higher stimulation frequencies generate lower firing rates in both fiber diameters (5.7 and 12.8 μm). Moreover, there are frequencies where the firing rate of a 5.7 μm nerve fiber is lower than the one of a 12.8 μm nerve fiber. For instance, in a 100 μs-stimuli, a 400 Hz-stimulus produced 400 Hz of firing rate in a 12.8 μm-diameter fiber while it is reduced by half (200 Hz) in a 5.7 μm-diameter fiber. In a 300 μs-stimuli, it is with a 600 Hz-stimulus when the firing rate of a 12.8 μm-diameter fiber is reduced by half (300 Hz) while it is one-third reduced in a 5.7 μm-diameter fiber (200 Hz). A similar effect is obtained with a 500 μs-stimuli 300 Hz-stimulus, where the firing rate of a 12.8 μm-diameter fiber is equivalent to the stimulation frequency (300 Hz), but the firing rate of a 5.7 μm-diameter fiber is reduced to one-third (200 Hz). Therefore, there are ranges of stimulation frequency where the neural activity of small nerve fibers is reduced, and the activity of the large axons is higher. For example, in a 100 μs-stimuli, the activity of large nerve fibers would be greater than small fibers at 375-425 Hz, 600-800 Hz, 900-1100 Hz, and 1100-1300 Hz. Instead, in a 500 μs-stimuli, the activity of large nerve fibers would be greater than small fibers at 200-400 Hz, and 600-800 Hz.

Fig. 8 also reveals that the higher the pulse width is, the firing rate is limited to a lower range of frequencies. Thus, a 100 μs-stimuli generates firing rates from 1 to 1300 Hz; a 300 μs-stimuli produces firing rates from 1 to 900 Hz; and the firing rate of a 500 μs-stimuli is produced between 1 and 775 Hz.

Fig. 9 shows the neural activity produced when applying a 300 μs, 350 Hz stimulus in 5.7 and 12.8 μm-diameter nerve fibers. In 12.8 μm nerve fiber, every pulse generates an action potential, while an action potential every two pulses is generated in 5.7 μm nerve fiber. At the second pulse, m (sodium channel) and n (potassium channel) gates are totally recovered in both nerve fiber diameters, however, the h gate (sodium channel) value is 0.496 (81.4% recovered) for the 12.8 μm-diameter fiber and 0.4676 (76.7% recovered) for the 5.7 μm-diameter fiber, i.e. the h gate recovery is faster in the 12.8 μm nerve fiber than in the 5.7 μm one. The threshold stimulus needed to activate both fibers is different. In this case, the threshold stimulus to activate a 5.7 μm-diameter fiber is 80% higher than the one for a 12.8 μm-diameter fiber (0.81 versus 0.45, respectively).

IV. DISCUSSION

A. NEW NERVE FIBER MODEL

This paper presents a new sensory nerve fiber that is a combination of the most used nerve fiber models in SCS modeling: a sensory nerve fiber model (the WHB model, which is the one that most approximates to human nerve fibers behavior [76]) and a motor nerve fiber model (the RMG model B, which is the one that most approximates to the real electrical behavior of the myelin [60]).

The main difference between the WHB model and the RMG model B is that they consider different ion channels. While the WHB model considers sodium, fast potassium, and leakage currents to have an approximate behavior of a human sensory nerve fibers, the RMG model B considers fast and persistent sodium current, slow potassium, and leakage

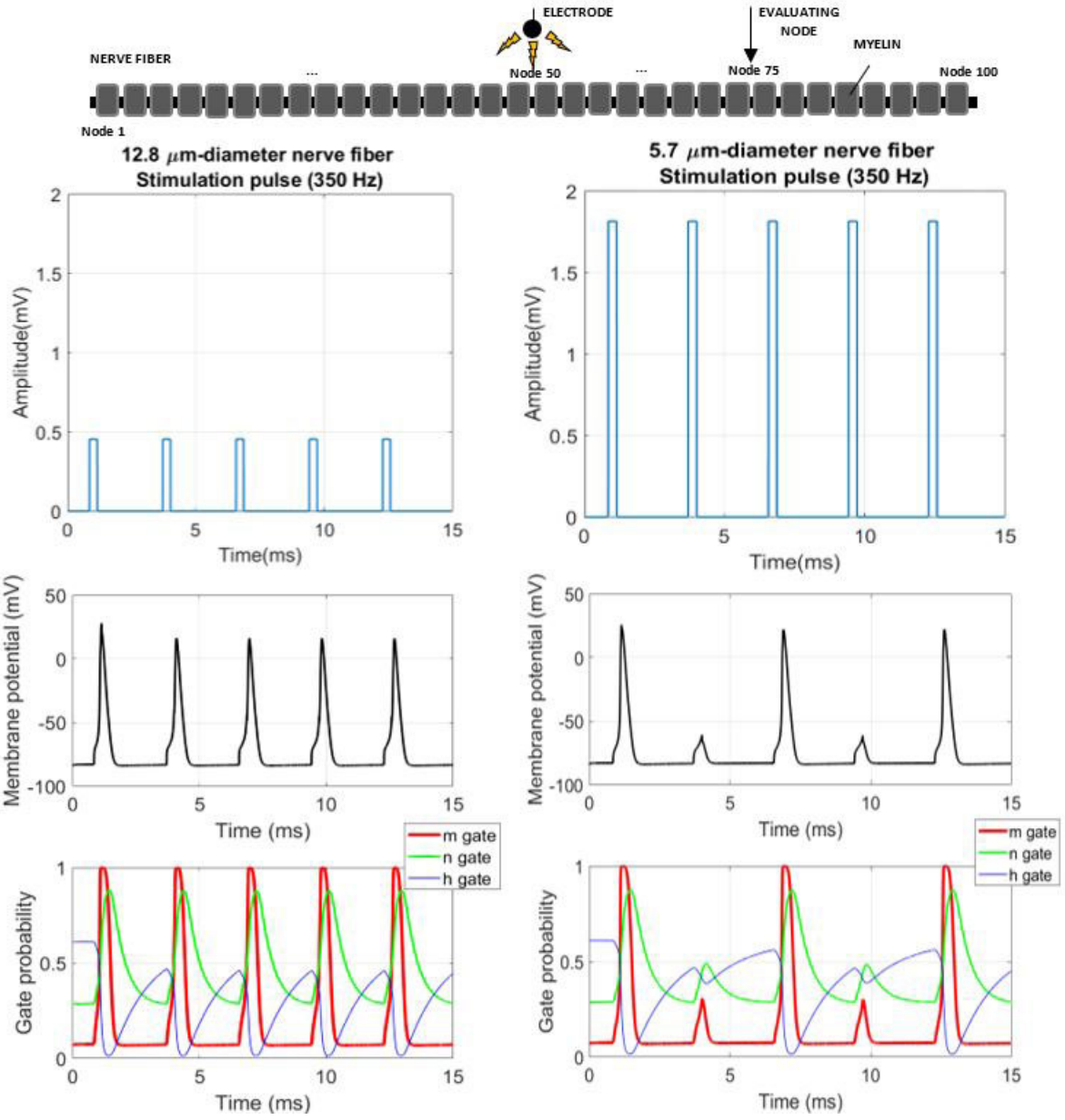

FIGURE 9. Electric response of a 12.8 μm nerve fiber (left) and 5.7 8 μm nerve fiber (right) during a stimulus with a frequency of 350 Hz and pulse width of 300 μs. The figures above show the stimulus pattern applied to 12.8 μm nerve fiber (left) and 5.7 μm nerve fiber (right). The figures of the right column show the action potential and the evolution of the gates' probabilities in the node 75 of the nerve fiber at each pulse stimulus. The amplitude applied is 1.2 V_{th} (threshold stimulus). Electrode is located at 0.5 mm from the middle of the axon.

currents with the aim of having an approximate behavior of mammalian motor nerve fibers. Moreover, they present a different myelin model; the WHB model considers the myelin as a perfect insulator, which is known to be an incorrect approximation, and thus a limitation of the model [47], [76]; and, otherwise, the RMG model B considers the myelin as an imperfect insulator, i.e. with current losses, which make the model more physiological accurate [60]. With the objective of having a more accurate sensory nerve fiber, a combination between these two models has been made. Thus, the new model maintains the same ion channels of the WHB model, and the myelin is modeled as in the RMG model B, i.e., as an imperfect insulator. Some model parameters were calibrated using action potential characteristics derived from physiological data and/or validated in previous computational studies.

To validate the electrical behavior of the new sensory nerve fiber model, we studied the shape and propagation of the action potential, the generation of afterpotentials, and the strength-duration and CV-diameter relationships.

We observed that amplitude, CV, chronaxie, absolute and relative refractory periods values obtained from the new model present a good approximation to experimental

data (see Table 2). The inclusion of the myelin as an imperfect insulator had significant changes in the fiber response. On the one hand, when the action potential is propagated to an internodal compartment, there is a decrease of the action potential amplitude, for this model considers current losses produced in the internodes of a myelinated nerve fiber. This effect produced a reduction of the CV, which is in concordance with McIntyre *et al.* [46]. On the other hand, the finite impedance myelin model considered also produced changes in the strength-duration and CV-diameter curves. From the strength-duration relationship results, the model developed presented a lower threshold stimulus than the WHB model. Furthermore, while the WHB had higher values than the MRG motor model for pulse durations below 200 μs, the model developed in this study showed lower values than the MRG motor fiber for all pulse durations. This outcome is in concordance with previous modeling results and experimental data [20], [21], [28], [45], [52], which show that sensory nerve fibers have lower stimulation thresholds than motor nerve fibers.

The CV-diameter curve also showed that the nerve fiber model of this study had lower CV values than the WHB sensory model for diameters above 8.7 μm. However, the CV obtained were within the experimental range from mammalian DC axons [59] and was also lower than the MRG motor nerve fiber, which is in accordance with Dawson *et al.* [15], who showed that sensory nerve fibers have lower CV than motor nerve fibers from human experimental data.

Moreover, we adjusted the voltage and time-dependent parameters of the sodium activation and inactivation coefficients. These changes avoided spontaneous firing and favored the generation of hyperpolarizing afterpotential following the action potential (see Fig. 3). However, no depolarizing afterpotentials were generated. Both depolarizing and hyperpolarizing afterpotentials can be produced in motor and sensory nerve fibers [46]. However, experimental recordings show that depolarizing afterpotentials are produced after the action potential in motor nerve fibers [14] while hyperpolarizing afterpotentials are produced after the action potential in sensory fibers [67]. According to previous studies [9], [43], [46], the afterpotential phenomena can extend tens of milliseconds after the action potential ($\sim$20 ms or more). Therefore, as the maximum timeframe of this study is 20 ms (in 50 Hz-stimulus), we can just consider the hyperpolarization after a spike that affects the refractory time of the nerve fiber model [5].

Hence, the agreement of the nerve fiber model behavior with experimental data made this computational model valid for the purpose of this study.

B. EFFECT OF FREQUENCY ON NERVE FIBER ACTIVATION

To investigate the role of frequency on neural activation, we simulated the action potential and the gates' probabilities at 50, 350, 600, 800, and 1000 Hz-stimulus, with a pulse width of 300 μs.

The results show that frequency is the stimulation parameter that allows us to increase or decrease the electrical activity of a sensory Aβ nerve fiber. Thus, while 50 Hz-stimulus produce a firing rate of 50 Hz in a 12.8 μm-diameter, the firing rate could be maximized to 350 by applying a 350 Hz-stimulus, since an action potential is obtained every pulse (see Fig. 5). North *et al.* stated that the stimulation rate of the neurons could be doubled by frequency doubling [55], which is in accordance with our results, since a higher stimulation frequency can increase the firing of large sensory Aβ nerve fibers. On the other hand, the results obtained in this study are also in agreement with the hypothetical neuron response stated by Miller *et al.* [50], who showed a neuron that would generate an action potential every three pulses when frequency was increased. As shown in Fig. 6, at 600-Hz pulse the nerve fiber fires every two pulses while it fires every third pulse at 800 Hz-stimulus. This outcome is in accordance with an experimental study, based on rat DC single axons recordings, from Crosby *et al.* [12], who showed that the increase of the kilohertz-frequency SCS from 1 to 20 kHz lowered the neuronal activity in the DC. Furthermore, according to Bowman and McNeal [7], stimulation frequencies higher than 1000 Hz generated a firing decrease and/or blockade of the action potential conduction of single alpha motoneurons from cats. This finding is also presented in Fig. 7, which shows how 1000 Hz-stimulus would override the electrical activation of a 12.8 μm-diameter nerve fiber (only an action potential is obtained at the first pulse). As for the gates' probabilities, the results show that m (sodium channel) gate recovers faster than n (potassium channel) and h (sodium) gates, playing an important role in nerve fiber depolarization, but not in repolarization. Although n and h gates participate in nerve fiber repolarization, the recovery is slower for h gate. Indeed, Fig. 5 and Fig. 6 show that the fiber cannot be depolarized until having h gate around 70-75% recovered. At 1000 Hz-stimulus (see Fig. 7), the time between pulses only allows h gate to recover a maximum of 68.72%, then no more action potentials are obtained after the first nerve depolarization. This outcome reveals that sodium channels, and more especifically the h gates, are responsible for the sensory nerve fiber excitability, which is in agreement with Bucher and Goaillard [8], who stated that the nerve fiber pattern activity is limited by the refractory period as well as the sodium channel inactivation. Another experimental study from Ackermann *et al.* [2] showed that fast sodium conductances play a role in determining the frequency at which the fiber was blocked. And a previous kilohertz-stimulation computational study from Arle *et al.* also stated that h gate was one of the primary ionic gate dynamics leading to high frequency blocking phenomena [5].

Therefore, the results of this study suggest that, in tonic stimulation, i.e., supra-threshold stimulation, low- (from 1 to 50 Hz), mid- (50-500 Hz), and high- (>500 Hz) frequency stimulation could have important implications in clinical practice. For instance, low-frequency would activate Aβ fibers at each pulse, yielding pain relief with a low duty cycle

(low energy consumption) [50], [65]. Mid-frequency would also produce Aβ fibers firing at each pulse up to 350 Hz, which would suppose the increase of Aβ neurons activity at the cost of increasing energy consumption. In this case, the cost-efficacy in terms of energy consumption of stimulation frequencies ranging from 50 to 350 Hz should be analyzed clinically to determine the stimulation frequency that is more efficient to produce pain relief. And high-frequency ($>$500 Hz), instead, would increase energy consumption without increasing sensory Aβ fibers firing, even going so far as to override the electrical activity of the sensory Aβ fibers (1000 Hz) [50].

On the other hand, not only does the stimulation pattern of an axon depend on the pulse frequency, but it also depends on the pulse width utilized and the size of the nerve fiber. As shown in Fig. 9, there are ranges of frequencies where the firing rate of large (12.8 μm-diameter) fibers is higher than the one of small (5.7 μm-diameter) fibers. This outcome demonstrate the hypothesis proposed by Miller *et al.* [50], who stated that the percentage of activated axons at any point in time would depend on the charge delivered as well as the depolarization and refractory period state. Moreover, Parker *et al.* provided direct electrophysiological evidence of recruitment of large-diameter, high-conduction-velocity Aβ sensory nerve fibers in the dorsal columns of the human spinal cord from measurements of evoked compound action potentials from patients undergoing SCS for pain relief [57]. According to Richardson *et al.* [60], variations in both the myelin conductance and capacitance (G_m and C_m) influence the excitation and conduction properties of the neuron, such as the chronaxie time, conduction velocity, or rheobase amplitude. As both the G_m and the C_m depend on the geometric parameters of the nerve fiber considered (see Appendix), the higher electrical response observed in the 12.8 μm-diameter fiber compared to the 5.7 μm-diameter fiber could be explained by the differences produced in the internodal parameters. Hence, as the refractory period is higher in small sensory fibers, it could be possible to modulate the neural activation of different neural structures to maximize the activity of the large Aβ neurons in SCS. This finding is in accordance with Mahmud and Vassanelli [44], who showed that the difference in membrane conductance properties of excitatory and inhibitory neurons allows modulating their firing by the stimulation wave parameters.

Besides, the results also show that the firing rate of a nerve fiber depends on the pulse width, since frequency and pulse width are inversely related when rectangular stimulation pulses are used [50]. Hitherto, the increase of pulse width produces lower firing rates, for the range of stimulation frequencies are also reduced (see Fig. 8).

Therefore, the knowledge of the electrical and geometrical properties of different neural structures, such as motoneurons, pyramidal neurons, sensory neurons, glial cells, etc., and the posterior development of computational neural models could help to better manage the frequency stimulation parameter to increase (or decrease) the activity of the targeted neural structures in a population of neurons, as stated by Jilge *et al.* [29].

In SCS therapy for chronic pain treatment, the stimulation protocols that are used in clinical practice can be divided into two groups: paresthesia-based SCS, known as tonic or ''low'' frequency stimulation; and paresthesia-free SCS, such as burst, high-frequency, and 10-kHz high-frequency SCS. While tonic stimulation uses supra-threshold stimulus and the mechanisms of action are well-known, the paresthesia-free protocols use sub-threshold stimulus, and the mechanisms of action are still unrevealed [11], [30], [73]. However, the advantage of paresthesia-free SCS is that patients can have pain relief without noticing the paresthesia sensation [3], [61]. In terms of energy cost, tonic stimulation is the most efficient, for it produces pain relief with the lowest duty cycle compared to burst or 10-kHz stimulation (4.6% versus 20 and 30%, respectively), as stated by Miller *et al.* [50]. Hence, the increase of alternative frequencies and stimulation patterns to improve patient's experience makes necessary the performance of computational studies that help us to understand the effect of the stimulation parameters for the better management of SCS therapy.

C. LIMITATIONS

In the new nerve fiber model, the myelin is modeled as a linear conductance in parallel with the membrane capacitance. There are more sophisticated sensory nerve fiber models developed, such as Howells *et al.* [28], Zhu *et al.* [77], and Gaines *et al.* [21], that include different segments (paranodal, juxtaparanodal, and internodal), in addition to ionic channels (fast K^+, slow K^+, leak, and hyperpolarization-activated cyclic-nucleotide gated (HCN)) in the internodes, which have a significant influence on the resting potential, and fiber accommodation [28]. Although these models are physiologically more accurate, the added computational complexity, and the parameter uncertainty of the dynamic behavior of the internodal channels they present justify the use of the simplified sensory nerve fiber model developed in this study [21], [46], [60]. Nonetheless, a recent study from Joosten and Franken [30] indicates that tonic SCS can depolarize the sensory Aβ fibers in both the antidromic and orthodromic directions. Antidromically, due to sensory Aβ fibers are branched, the inhibitory interneurons located in the dorsal horn can be activated, inhibiting then the incoming signals from nociceptors and thus closing the ''spinal gate of pain''. Therefore, future sensory nerve fiber models should include branch points since it could increase the accuracy of the model-based predictions when investigating the excitability of sensory Aβ nerve fibers.

This work is focused on the simulation of the effect of frequency on neural activation in tonic stimulation. It is well-known that stimulation frequencies ranging between 40-60 Hz produce paresthesia and increase GABA neurotransmitter release from GABAergic inhibitory interneurons that are activated by Aβ fibers inputs, according to the gate-control mechanism of action [22]. However,

higher frequencies seem to produce other mechanisms that help to relief neuropathic pain, such as 100 Hz, that likely activates endogenous δ-opioid systems; or 500 Hz, that was shown to improve peripheral blood flow [22], [50]. Our nerve fiber model does not consider any transsynaptic network processing nor any neurotransmitters release, which are known processes involved in the tonic SCS mechanisms of action [30]. Thus, the real clinical effects could differ from the clinical implications exposed from the results of this work.

A recent computational study from Arle *et al.* [4] shows that threshold accommodation is higher in the large-diameter fibers than in the small ones, yielding thus the inversion of larger and smaller diameter fiber thresholds. Unlike tonic spinal cord stimulation, the accommodation phenomenon could suppose the recruitment of smaller DC fibers (medium-diameter fibers) in burst stimulation and high-frequency stimulation, which could explain the paresthesia-free mechanism of action treatments [4]. Fiber accommodation phenomenon is produced after applying a single or a train of conditioning pulses, which help us to investigate the fiber's excitability [4], [28], [40], [41]. Owing to conditioning pulses are not used in SCS therapy, nor are different stimulus pulses applied simultaneously, we did not analyze the threshold accommodation phenomenon in this work. Nonetheless, future computational studies that use conditioning stimulus should consider this effect to investigate the influence of fiber accommodation.

The effect of the stimulation amplitude to different stimulation frequencies on the neuronal activation pattern was not included in this study. According to Miller *et al.* [50], the amplitude should be considered when discussing the neural mechanisms of SCS frequency. For example, with moderate-high amplitude, the high frequency could induce axonal blocking mechanisms, while subthreshold stimulation could favor non-activating neuronal mechanisms, such as temporal summation, or desynchronization of the neural activity [32], [37]. Thus, future computational studies related to the effect of frequency on neural response in SCS therapy for chronic pain treatment should include the influence of the stimulation amplitude.

The findings of this computational study are based on the electrical response of a single sensory Aβ nerve fiber under extracellular stimulation. Although the outcome of this work has been extrapolated to possible clinical implications in tonic SCS, both a computational study using a realistic SCS model, and a clinical study related to the effect of the stimulation frequency in tonic SCS should be performed to validate the results. The nerve fiber distribution in the dorsal columns, the electrical properties of the spinal cord, and the different spinal elements involved in the mechanisms of action of tonic SCS are elements that should be considered in future research works to increase the accuracy of the model-based predictions in SCS therapy.

V. CONCLUSION

We developed a new sensory nerve fiber model which is physiologically accurate and simulates the behavior of human sensory nerve fibers. The findings of this computational study suggest that in tonic SCS for chronic pain treatment, large sensory Aβ fibers activity can be risen by increasing the stimulation frequency up to 350 Hz. On the contrary, frequencies from 350 to 1000 Hz would decrease sensory fibers firing, or even override it, with an additional increase of energy consumption. Moreover, the outcomes show that frequency can also increase large sensory fibers activity while decreasing small sensory fibers, suggesting that frequency plays an important role to modulate the firing rate of a nerve fiber size. Thereby, according to our results, frequency could be a stimulation parameter that would allow us to select and increase the activity of a specific neural structure.

APPENDIX

The new sensory nerve fiber model and its parameters at body temperature (37°C).

Fiber geometry parameters [46]:

D: axon diameter (cm)

F_d: fiber diameter (cm)

L: internodal length (cm)

l: nodal length (cm) (its value is $1{\cdot}10^{-4}$)

d: nodal diameter (cm) (value depends on fiber diameter)

lam_{memb}: number of myelin lamellas (value depends on fiber diameter)

lam: number of lamella membranes per lamella (its value is 2)

$$D = C_d F_d - D_d$$
$$L = C_L log(D \cdot (D_L)^{-1})$$

where $C_d = 0.76$, $D_d = 1.81 \cdot 10^{-6}$, $C_L = 7.87 \cdot 10^{-4}$, and $D_L = 3.44 \cdot 10^{-6}$.

The parameters d and lam depend on fiber diameter as follows [46]:

Fiber diameter (μm)	d (μm)	lam
5.7	1.9	80
12.8	4.2	135

Gating parameters [76]:

Sodium m gates activation (α_m is taken from Howells *et al.* [28]):

$$\alpha_m = [3.13 \cdot 10^3 (V_m + 36.3)]/[1 - e^{(-36.3 - V_m)/10.3}]$$
$$\beta_m = [0.33 \cdot 10^3 (-22.7 - V_m)]/[1 - e^{(V_m + 22.7)/9.16}]$$

Sodium h gates activation (α_h is taken from Howells *et al.* [28]):

$$\alpha_h = [0.153 \cdot 10^3 (-113.8 - V_m)]/[1 - e^{(V_m + 113.8)/11.9}]$$
$$\beta_h = [14.1 \cdot 10^3/[1 + e^{(-28.8 - V_m)/13.4}]$$

Potassium n gates activation:

$$\alpha_n = [51.7(V_m + 93.2)]/[1 - e^{(-93.2-V_m)/1.1}]$$
$$\beta_n = [92(-76 - V_m)]/[1 - e^{(V_m+76)/10.5}]$$

Membrane potential V_m in millivolts (mV)
Canonical gate probability equation:

$$\frac{d\omega}{dt} = \alpha_\omega(1 - \omega) - \beta_\omega\omega$$

where $\omega = m, h, n$ and the initial conditions (when $t = 0$) are:

$$m(0) = 0.07427$$
$$h(0) = 0.6096$$
$$n(0) = 0.2873$$

Internode parameters [60]:
C_m: Myelin capacitance (mF)
G_m Myelin conductance (mS)
C_n: Nodal capacitance (mF)
G_a: Conductance between compartments (mS)

$$C_m = (c_m\pi F_d L)(lam \cdot lam_{memb})^{-1}$$
$$G_m = (g_m\pi F_d L)(lam \cdot lam_{memb})^{-1}$$
$$C_n = c_n\pi dl$$
$$G_a = (\pi D^2)(4\rho_{ax}L)^{-1}$$

Membrane currents [76]:
i_{Na}: Sodium channel current density (mA/cm^2)
i_K: Fast potassium channel current density (mA/cm^2)
i_{Lk}: Leak channel current density (mA/cm^2)
I_{ion}: Total ion current (mA/cm^2)

$$i_{Na} = (p_{Na}m^3\, hVF^2([Na]_o - [Na]_i e^{\frac{VF}{RT}}))(RT(1 - e^{\frac{VF}{RT}}))^{-1}$$
$$i_K = n^4\, g_K(V_m - E_K)$$
$$i_{Lk} = g_{Lk}(V_m - E_{Lk})$$
$$I_{ion} = i_{Na} + i_{Ks} + i_{Lk}$$

The sodium equilibrium potential (E_{Na}) can be calculated applying the Nerst equation:

$$E_{Na} = \frac{RT}{F} \ln \frac{[Na]_o}{[Na]_i} \quad (3)$$

REFERENCES

[1] D. Abejón, P. Rueda, J. del Saz, S. Arango, E. Monzón, and F. Gilsanz, "Is the introduction of another variable to the strength-duration curve necessary in neurostimulation?" *Neuromodulation, Technol. Neural Interface*, vol. 18, no. 3, pp. 182–190, Apr. 2015.
[2] D. M. Ackermann, Jr., N. Bhadra, M. Gerges, and P. J. Thomas, "Dynamics and sensitivity analysis of high-frequency conduction block," *J. Neural Eng.*, vol. 8, no. 6, 2011, Art. no. 065007.
[3] S. Ahmed, T. Yearwood, D. De Ridder, and S. Vanneste, "Burst and high frequency stimulation: Underlying mechanism of action," *Expert Rev. Med. Devices*, vol. 15, no. 1, pp. 61–70, Jan. 2018.
[4] J. E. Arle, L. Mei, and K. W. Carlson, "Fiber threshold accommodation as a mechanism of burst and high-frequency spinal cord stimulation," *Neuromodulation, Technol. Neural Interface*, vol. 23, no. 5, pp. 582–593, Jul. 2020.
[5] J. E. Arle, L. Mei, K. W. Carlson, and J. L. Shils, "High-frequency stimulation of dorsal column axons: Potential underlying mechanism of paresthesia-free neuropathic pain relief," *Neuromodulation, Technol. Neural Interface*, vol. 19, no. 4, pp. 385–397, Jun. 2016.
[6] B. P. Bean, "The action potential in mammalian central neurons," *Nature Rev. Neurosci.*, vol. 8, no. 6, pp. 451–465, 2007.
[7] B. R. Bowman and D. R. McNeal, "Response of single alpha motoneurons to high-frequency pulse trains," *Stereotactic Funct. Neurosurg.*, vol. 49, no. 3, pp. 121–138, 1987.
[8] D. Bucher and J.-M. Goaillard, "Beyond faithful conduction: Short-term dynamics, neuromodulation, and long-term regulation of spike propagation in the axon," *Prog. Neurobiol.*, vol. 94, no. 4, pp. 307–346, Sep. 2011.
[9] D. Burke, M. C. Kiernan, and H. Bostock, "Excitability of human axons," *Clin. Neurophysiol.*, vol. 112, no. 9, pp. 1575–1585, Sep. 2001.
[10] M. R. Carhart, J. He, R. Herman, S. D'Luzansky, and W. T. Willis, "Epidural spinal-cord stimulation facilitates recovery of functional walking following incomplete spinal-cord injury," *IEEE Trans. Neural Syst. Rehabil. Eng.*, vol. 12, no. 1, pp. 32–42, Mar. 2004.
[11] J. Caylor, R. Reddy, S. Yin, C. Cui, M. Huang, C. Huang, R. Rao, D. G. Baker, A. Simmons, D. Souza, S. Narouze, R. Vallejo, and I. Lerman, "Spinal cord stimulation in chronic pain: Evidence and theory for mechanisms of action," *Bioelectron. Med.*, vol. 5, no. 1, p. 12, Dec. 2019.
[12] N. D. Crosby, J. J. Janik, and W. M. Grill, "Modulation of activity and conduction in single dorsal column axons by kilohertz-frequency spinal cord stimulation," *J. Neurophysiol.*, vol. 117, no. 1, pp. 136–147, Jan. 2017.
[13] D. Darrow, D. Balser, T. I. Netoff, A. Krassioukov, A. Phillips, A. Parr, and U. Samadani, "Epidural spinal cord stimulation facilitates immediate restoration of dormant motor and autonomic supraspinal pathways after chronic neurologically complete spinal cord injury," *J. Neurotrauma*, vol. 36, no. 15, pp. 2325–2336, Aug. 2019.
[14] G. David, B. Modney, K. A. Scappaticci, J. N. Barrett, and E. F. Barrett, "Electrical and morphological factors influencing the depolarizing afterpotential in rat and lizard myelinated axons," *J. Physiol.*, vol. 489, no. 1, pp. 141–157, Nov. 1995.
[15] G. D. Dawson, "The relative excitability and conduction velocity of sensory and motor nerve fibres in man," *J. Physiol.*, vol. 131, no. 2, pp. 436–451, Feb. 1956.
[16] D. De Ridder, M. Plazier, N. Kamerling, T. Menovsky, and S. Vanneste, "Burst spinal cord stimulation for limb and back pain," *World Neurosurg.*, vol. 80, no. 5, pp. 642–649, 2013.
[17] J. L. Durá, C. Solanes, J. De Andrés, and J. Saiz, "Computational study of the effect of electrode polarity on neural activation related to paresthesia coverage in spinal cord stimulation therapy," *Neuromodulation, Technol. Neural Interface*, vol. 22, no. 3, pp. 269–279, Apr. 2019.
[18] H. K. P. Feirabend, H. Choufoer, S. Ploeger, J. Holsheimer, and J. D. van Gool, "Morphometry of human superficial dorsal and dorsolateral column fibres: Significance to spinal cord stimulation," *Brain*, vol. 125, no. 5, pp. 1137–1149, May 2002.
[19] D. Fiume, "Spinal cord stimulation in peripheral vascular pain," *Stereotactic Funct. Neurosurg.*, vol. 46, nos. 5–6, pp. 290–294, 1983.
[20] J. C. Forst, D. C. Blok, J. P. Slopsema, J. M. Boss, L. A. Heyboer, C. M. Tobias, and K. H. Polasek, "Surface electrical stimulation to evoke referred sensation," *J. Rehabil. Res. Develop.*, vol. 52, no. 4, pp. 397–406, 2015.
[21] J. L. Gaines, K. E. Finn, J. P. Slopsema, L. A. Heyboer, and K. H. Polasek, "A model of motor and sensory axon activation in the median nerve using surface electrical stimulation," *J. Comput. Neurosci.*, vol. 45, no. 1, pp. 29–43, Aug. 2018.
[22] Y. Guan, "Spinal cord stimulation: Neurophysiological and neurochemical mechanisms of action," *Current Pain Headache Rep.*, vol. 16, no. 3, pp. 217–225, Jun. 2012.
[23] S. Harkema, Y. Gerasimenko, J. Hodes, J. Burdick, C. Angeli, Y. Chen, C. Ferreira, A. Willhite, E. Rejc, R. G. Grossman, and V. R. Edgerton, "Effect of epidural stimulation of the lumbosacral spinal cord on voluntary movement, standing, and assisted stepping after motor complete paraplegia: A case study," *Lancet*, vol. 377, pp. 1938–1947, Jun. 2011.
[24] T. L. Yearwood, "Pulse width programming in spinal cord stimulation: A clinical study," *Pain Physician*, vol. 13, no. 7, pp. 321–335, Jul. 2010.
[25] J. Holsheimef and G. Barolat, "Spinal geometry and paresthesia coverage in spinal cord stimulation," *Neuromodulation, Technol. Neural Interface*, vol. 1, no. 3, pp. 129–136, Jul. 1998.
[26] J. Holsheimer, "Which neuronal elements are activated directly by spinal cord stimulation," *Neuromodulation, Technol. Neural Interface*, vol. 5, no. 1, pp. 25–31, Jan. 2002.

[27] J. Holsheimer and W. A. Wesselink, "Effect of anode-cathode configuration on paresthesia coverage in spinal cord stimulation," *Neurosurgery*, vol. 41, no. 3, pp. 654–660, Sep. 1997.
[28] J. Howells, L. Trevillion, H. Bostock, and D. Burke, "The voltage dependence of Ih in human myelinated axons," *J. Physiol.*, vol. 590, no. 7, pp. 1625–1640, Apr. 2012.
[29] B. Jilge, K. Minassian, F. Rattay, and M. R. Dimitrijevic, "Frequency-dependent selection of alternative spinal pathways with common periodic sensory input," *Biol. Cybern.*, vol. 91, no. 6, pp. 359–376, Dec. 2004.
[30] E. A. Joosten and G. Franken, "Spinal cord stimulation in chronic neuropathic pain: Mechanisms of action, new locations, new paradigms," *Pain*, vol. 161, no. 1, pp. S104–S113, 2020.
[31] L. Kapural, C. Yu, M. W. Doust, B. E. Gliner, R. Vallejo, B. T. Sitzman, K. Amirdelfan, D. M. Morgan, L. L. Brown, T. L. Yearwood, R. Bundschu, A. W. Burton, T. Yang, R. Benyamin, and A. H. Burgher, "Novel 10-kHz high-frequency therapy (HF10 therapy) is superior to traditional low-frequency spinal cord stimulation for the treatment of chronic back and leg pain: The SENZA-RCT randomized controlled trial," *Anesthesiology*, vol. 123, no. 4, pp. 851–860, 2015.
[32] K. L. Kilgore and N. Bhadra, "Reversible nerve conduction block using kilohertz frequency alternating current," *Neuromodulation, Technol. Neural Interface*, vol. 17, no. 3, pp. 242–255, Aug. 2013.
[33] K. Kumar, S. Rizvi, and S. B. Bnurs, "Spinal cord stimulation is effective in management of complex regional pain syndrome I: Fact or fiction," *Neurosurgery*, vol. 69, no. 3, pp. 566–580, Sep. 2011.
[34] K. Kumar, R. S. Taylor, L. Jacques, S. Eldabe, M. Meglio, J. Molet, S. Thomson, J. O'Callaghan, E. Eisenberg, G. Milbouw, E. Buchser, G. Fortini, J. Richardson, and R. B. North, "Spinal cord stimulation versus conventional medical management for neuropathic pain: A multicentre randomised controlled trial in patients with failed back surgery syndrome," *Pain*, vol. 132, no. 1, pp. 179–188, 2007.
[35] A. W. Lee and J. G. Pilitsis, "Spinal cord stimulation: Indications and outcomes," *Neurosurgical Focus*, vol. 21, no. 6, pp. 1–6, Dec. 2006.
[36] D. Lee, B. Hershey, K. Bradley, and T. Yearwood, "Predicted effects of pulse width programming in spinal cord stimulation: A mathematical modeling study," *Med. Biol. Eng. Comput.*, vol. 49, no. 7, p. 765, Jul. 2011.
[37] S. F. Lempka, C. C. McIntyre, K. L. Kilgore, and A. G. Machado, "Computational analysis of kilohertz frequency spinal cord stimulation for chronic pain management," *Anesthesiology*, vol. 122, no. 6, pp. 1362–1376, Jun. 2015.
[38] S. F. Lempka and P. G. Patil, "Innovations in spinal cord stimulation for pain," *Current Opinion Biomed. Eng.*, vol. 8, pp. 51–60, Dec. 2018.
[39] S. F. Lempka, H. J. Zander, C. J. Anaya, A. Wyant, J. G. Ozinga, and A. G. Machado, "Patient-specific analysis of neural activation during spinal cord stimulation for pain," *Neuromodulation, Technol. Neural Interface*, vol. 23, no. 5, pp. 572–581, Jul. 2020.
[40] C. S.-Y. Lin, I. Mogyoros, and D. Burke, "Recovery of excitability of cutaneous afferents in the median and sural nerves following activity," *Muscle Nerve*, vol. 23, no. 5, pp. 763–770, May 2000.
[41] C. S. Lin, I. Mogyoros, S. Kuwabara, C. Cappelen-Smith, and D. Burke, "Accommodation to depolarizing and hyperpolarizing currents in cutaneous afferents of the human median and sural nerves," *J. Physiol.*, vol. 529, no. 2, p. 483, 2000.
[42] B. Linderoth and R. D. Foreman, "Conventional and novel spinal stimulation algorithms: Hypothetical mechanisms of action and comments on outcomes," *Neuromodulation, Technol. Neural Interface*, vol. 20, no. 6, pp. 525–533, Aug. 2017.
[43] H. Liu, J. R. Roppolo, W. C. de Groat, and C. Tai, "The role of slow potassium current in nerve conduction block induced by high-frequency biphasic electrical current," *IEEE Trans. Biomed. Eng.*, vol. 56, no. 1, pp. 137–146, Oct. 2008.
[44] M. Mahmud and S. Vassanelli, "Differential modulation of excitatory and inhibitory neurons during periodic stimulation," *Frontiers Neurosci.*, vol. 10, p. 62, Feb. 2016.
[45] P. G. S. Makker, J. M. Matamala, S. B. Park, J. G. Lees, M. C. Kiernan, D. Burke, G. Moalem-Taylor, and J. Howells, "A unified model of the excitability of mouse sensory and motor axons," *J. Peripheral Nervous Syst.*, vol. 23, no. 3, pp. 159–173, Sep. 2018.
[46] C. C. McIntyre, A. G. Richardson, and W. M. Grill, "Modeling the excitability of mammalian nerve fibers: Influence of afterpotentials on the recovery cycle," *J. Neurophysiol.*, vol. 87, no. 2, pp. 995–1006, Feb. 2002.
[47] D. R. McNeal, "Analysis of a model for excitation of myelinated nerve," *IEEE Trans. Biomed. Eng.*, vol. BME-23, no. 4, pp. 329–337, Jul. 1976.
[48] N. A. Mekhail, M. Mathews, F. Nageeb, M. Guirguis, M. N. Mekhail, and J. Cheng, "Retrospective review of 707 cases of spinal cord stimulation: Indications and complications," *Pain Pract.*, vol. 11, no. 2, pp. 148–153, Mar. 2011.
[49] R. Melzack and P. D. Wall, "Pain mechanisms: A new theory," *Science*, vol. 150, no. 3699, pp. 971–979, 1965.
[50] J. P. Miller, S. Eldabe, E. Buchser, L. M. Johanek, Y. Guan, and B. Linderoth, "Parameters of spinal cord stimulation and their role in electrical charge delivery: A review," *Neuromodulation, Technol. Neural Interface*, vol. 19, no. 4, pp. 373–384, Jun. 2016.
[51] X. Min, A. R. Kent, S. P. Rosenberg, and T. A. Fayram, "Modeling dermatome selectivity of single- and multiple-current source spinal cord stimulation systems," in *Proc. 36th Annu. Int. Conf. IEEE Eng. Med. Biol. Soc.*, Aug. 2014, pp. 6246–6249.
[52] I. Mogyoros, M. C. Kiernan, and D. Burke, "Strength-duration properties of human peripheral nerve," *Brain*, vol. 119, no. 2, pp. 439–447, 1996.
[53] G. Molnar and G. Barolat, "Principles of cord activation during spinal cord stimulation," *Neuromodulation, Technol. Neural Interface*, vol. 17, pp. 12–21, Jun. 2014.
[54] G. Morita, Y. X. Tu, Y. Okajima, S. Honda, and Y. Tomita, "Estimation of the conduction velocity distribution of human sensory nerve fibers," *J. Electromyogr. Kinesiol.*, vol. 12, no. 1, pp. 37–43, Feb. 2002.
[55] R. B. North, D. H. Kidd, J. Olin, J. M. Sieracki, and M. Boulay, "Spinal cord stimulation with interleaved pulses: A randomized, controlled trial," *Neuromodulation, Technol. Neural Interface*, vol. 10, no. 4, pp. 349–357, Oct. 2007.
[56] L. G. Nowak and J. Bullier, "Axons, but not cell bodies, are activated by electrical stimulation in cortical gray matter," *Exp. Brain Res.*, vol. 118, no. 4, pp. 477–488, Feb. 1998.
[57] J. L. Parker, D. M. Karantonis, P. S. Single, M. Obradovic, and M. J. Cousins, "Compound action potentials recorded in the human spinal cord during neurostimulation for pain relief," *Pain*, vol. 153, no. 3, pp. 593–601, 2012.
[58] J. E. Pope, S. Falowski, and T. R. Deer, "Advanced waveforms and frequency with spinal cord stimulation: Burst and high-frequency energy delivery," *Expert Rev. Med. Devices*, vol. 12, no. 4, pp. 431–437, Jul. 2015.
[59] J. B. Ranck, "Which elements are excited in electrical stimulation of mammalian central nervous system: A review," *Brain Res.*, vol. 98, no. 3, pp. 417–440, Nov. 1975.
[60] A. G. Richardson, C. C. McIntyre, and W. M. Grill, "Modelling the effects of electric fields on nerve fibres: Influence of the myelin sheath," *Med. Biol. Eng. Comput.*, vol. 38, no. 4, pp. 438–446, Jul. 2000.
[61] M. Russo and J.-P. Van Buyten, "10-kHz high-frequency SCS therapy: A clinical summary," *Pain Med.*, vol. 16, no. 5, pp. 934–942, May 2015.
[62] S. Saeed and M. Akram, "Impact of anthropometric measures on sural nerve conduction in healthy subjects," *J. Ayub Med. College Abbottabad*, vol. 20, no. 4, p. 112, 2008.
[63] G. Schalow, G. A. Zäch, and R. Warzok, "Classification of human peripheral nerve fibre groups by conduction velocity and nerve fibre diameter is preserved following spinal cord lesion," *J. Autonomic Nervous Syst.*, vol. 52, nos. 2–3, pp. 125–150, Apr. 1995.
[64] J. R. Schwarz, G. Reid, and H. Bostock, "Action potentials and membrane currents in the human node of Ranvier," *Pflügers Archiv Eur. J. Physiol.*, vol. 430, no. 2, pp. 283–292, Jun. 1995.
[65] K. Shimoji, M. Matsuki, H. Shimizu, T. Iwane, R. Takahashi, M. Maruyama, and K. Masuko, "Low-frequency, weak extradural stimulation in the management of intractable pain," *Brit. J. Anaesthesia*, vol. 49, no. 11, pp. 1081–1086, Nov. 1977.
[66] B. Simpson, "Spinal cord stimulation in 60 cases of intractable pain," *J. Neurol., Neurosurg. Psychiatry*, vol. 54, no. 3, pp. 196–199, 1991.
[67] M. J. Stebbing, S. Eschenfelder, H.-J. Häbler, M. C. Acosta, W. Jänig, and E. M. McLachlan, "Changes in the action potential in sensory neurones after peripheral axotomy *in vivo*," *NeuroReport*, vol. 10, no. 2, pp. 201–206, Feb. 1999.
[68] J. J. Struijk, J. Holsheimer, G. G. van der Heide, and H. B. K. Boom, "Recruitment of dorsal column fibers in spinal cord stimulation: Influence of collateral branching," *IEEE Trans. Biomed. Eng.*, vol. 39, no. 9, pp. 903–912, Sep. 1992.
[69] W. Tackmann and H. J. Lehmann, "Refractory period in human sensory nerve fibres," *Eur. Neurol.*, vol. 12, nos. 5–6, pp. 277–292, 1974.
[70] T. Tateno, A. Harsch, and H. Robinson, "Threshold firing frequency–current relationships of neurons in rat somatosensory cortex: Type 1 and type 2 dynamics," *J. Neurophysiol.*, vol. 92, no. 4, pp. 2283–2294, 2004.

[71] R. S. Taylor, J. Ryan, R. O'Donnell, S. Eldabe, K. Kumar, and R. B. North, "The cost-effectiveness of spinal cord stimulation in the treatment of failed back surgery syndrome," *Clin. J. Pain*, vol. 26, no. 6, pp. 463–469, 2010.
[72] J. Tiede, L. Brown, G. Gekht, R. Vallejo, T. Yearwood, and D. Morgan, "Novel spinal cord stimulation parameters in patients with predominant back pain," *Neuromodulation, Technol. Neural Interface*, vol. 16, no. 4, pp. 370–375, Jul. 2013.
[73] R. Vallejo, K. Bradley, and L. Kapural, "Spinal cord stimulation in chronic pain," *Spine*, vol. 42, no. 1, pp. S53–S60, 2017.
[74] B. K. van Veen, R. L. L. A. Schellens, D. F. Stegeman, R. Schoonhoven, and A. A. W. M. Gabreëls-Festen, "Conduction velocity distributions compared to fiber size distributions in normal human sural nerve," *Muscle Nerve*, vol. 18, no. 10, pp. 1121–1127, Oct. 1995.
[75] P. Verrills, C. Sinclair, and A. Barnard, "A review of spinal cord stimulation systems for chronic pain," *J. Pain Res.*, vol. 9, p. 481, Jul. 2016.
[76] W. A. Wesselink, J. Holsheimer, and H. B. K. Boom, "A model of the electrical behaviour of myelinated sensory nerve fibres based on human data," *Med. Biol. Eng. Comput.*, vol. 37, no. 2, pp. 228–235, Mar. 1999.
[77] K. Zhu, L. Li, X. Wei, and X. Sui, "A 3D computational model of transcutaneous electrical nerve stimulation for estimating Aβ tactile nerve fiber excitability," *Frontiers Neurosci.*, vol. 11, p. 250, May 2017.

CARMEN SOLANES was born in Cullera, Valencia, Spain, in 1994. She received the B.Sc. and M.Sc. degrees in biomedical engineering from the Universitat Politècnica de València (UPV), Valencia, in 2016 and 2017, respectively, where she is currently pursuing the Ph.D. degree in technologies for health and well-being.

Since 2017, she has been working as a Biomedical Engineer at Biotecnología y Salud S.L., Valencia, where she works on giving technical assistance to physicians in spinal cord stimulation, drug infusion pumps, deep brain stimulation surgeries, and programming medical devices for neurological diseases treatment. Her research interests include spinal cord stimulation modeling and simulation, the development of patient-specific spinal cord models, and fundamental study of the effect of the stimulation parameters on neural activation.

JOSÉ L. DURÁ (Member, IEEE) was born in Valencia, Spain, in 1965. He received the M.Sc. degree in mechanical engineering from the Universitat Politècnica de València (UPV), Valencia, in 1989, where he is currently pursuing the Ph.D. degree in technologies for health and well-being.

From 1989 to 1996, he was working in cardiology at ELA Medical, Montrouge, France, and cardiac valves at Medical Inc., Minneapolis, MN, USA. From 1996 to 2008, he worked at Medtronic Iberica S.A., Madrid, Spain, as a Product Manager with Neuromodulation Division. Since 2008, he has been a CEO and a Founder of surgical engineering at Surgicen, Valencia, a company providing bioengineering services. His research interests include spinal cord stimulation and the design and development of new devices.

JOSE DE ANDRÉS received the M.D. degree from the School of Medicine, Valencia University.

He is currently a tenured Professor of anaesthesiology with the School of Medicine, Valencia University. After stays at several eminent hospitals, he is based at General University Hospital, Valencia, Spain, where he holds the positions of the Chairman of Anaesthesia, Critical Care, and of the Multidisciplinary Pain Management Departments. He has a special interests include the prevention and management of pain, from acute postoperative pain to chronic pain syndromes. He is involved in ongoing research in pain and current areas of investigation include the expression of pain and its control through neuromodulation techniques, neuroimaging markers, and genomic expression, in addition to the computerized prediction designs of programming models and design of neuromodulation systems. His expertise has led to the publication of numerous articles, with accumulated impact factor: 296 745; index H of Hirsch: 28; average citations per item: 15,3; and average citations per year: 45,8.

Dr. De Andrés has been a Committee Member of "Society Liaison and Advocacy" International Neuromodulation Society (INS), since 2016. He received frequent invitations to chair or present at international symposia, lectures, and conferences. He received academic six-year term research award (so-called sexenium) (1994–2017). He is the Vice-Chairman of European Society of Regional Anesthesia and Pain Therapy (ESRA) to obtain the European Diploma of Chronic Pain Management (EDPM). He is on the editorial boards of several national and international journals as *Pain Practice*, *European Journal of Pain*, *Regional Anesthesia and Pain Medicine*, and *The Clinical Journal of Pain*.

JAVIER SAIZ was born in Valencia, Spain, in 1960. He received the Ph.D. degree from the Universitat Politècnica de València (UPV), Valencia, in 1992.

In 1995 and 2010, he was a Postdoctoral Research Fellow at Johns Hopkins University, Baltimore, USA., and Oxford University, Oxford, GB. He is currently a Full Professor with the Department of Electronic and the Director of the Center of Research and Innovation in Bioengineering (Ci2B), UPV. He is the author of more than 80 articles. His research interests include cardiac and neural electrophysiology, computer modeling of electrical propagation in cells, tissues and organs, electrical stimulation, modeling of drug-ion channel interactions, biomedical signal processing, and medical instrumentation.

Prof. Saiz has been a member of the Royal Academy of Medicine of the Valencian Community, since November 2017.